$\mathcal{H}_\infty$ Robust Controller for a Long VSC-HVDC Link Connected to a Weak Grid

نظام تحكم متين لخط نقل جهد عالى مستمر طويل ذو محولات منابع الجهد متصل بشبكة ضعيفة

Mohamed Rashed, *Member, IEEE, IET*, S. Abulanwar and Fathi M. H. Youssef
Electrical Engineering Department, Mansoura University, Mansoura 35516, Egypt

ملخص

نظرا للأداء الديناميكي العالى ومرونة التحكم فإن أنظمة نقل التيار المستمر توجد على نطاق واسع فى شبكات القوى وذلك لتحسين الخصائص الديناميكية. هذا البحث يقدم نظام تحكم متين غير مركزى للنظام نقل تيار مستمر يستخدم لربط شبكة ضعيفة بشبكة قوية من خلال كابل طويل. تستخدم طريقة التحكم المتين لتصميم نظام التحكم للشبكة الضعيفة وذلك لتحقيق اتزان متين وأداء ديناميكى فائق تحت مدى تغير كبير لنسبة القصر للشبكة الضعيفة. تستخدم طريقة الإشارة الصغيرة وتحليل استجابة الخطوة لتصميم نظام التحكم تحت ظروف تشغيل مختلفة وتغير لنسبة القصر. علاوة على ذلك يتم مقارنة أداء نظام التحكم المتين مع نظام تحكم تكاملى متناسب مصمم جيدا. النتائج التي تم الحصول عليها تعطي أداء ديناميكي متين تحت ظروف تشغيل مختلفة وتغير للنسبة القصر.

Abstract: **Owing to their high dynamic performance and flexible control features, HVDC systems are widely employed in power systems for dynamic characteristics improvement. This paper presents a decentralized robust control scheme for a VSC-HVDC transmission system. The VSC-HVDC system is used to connect a weak AC gird to a strong power system using a long DC link. The robust multivariable H-infinity $\mathcal{H}_\infty$ control approach is adopted for the design of the weak grid side controller in order to achieve robust stability and superior dynamic performance under large uncertainty in the short circuit ratio SCR of the weak grid. Small-signal modeling and step response analysis are used to design the system controllers under different operating conditions and wide range of SCR variation. Furthermore, the $\mathcal{H}_\infty$ control system results are compared to that of a well designed PI based control system. The obtained results demonstrate robust dynamic performance under various operating conditions and large SCR variation.**

Keywords: VSC-HVDC, Weak Grid, Robust Control.

I. Introduction

High voltage direct current (HVDC) transmission systems based voltage source converters (VSC-HVDC) is a new electrical transmission system that has attracted more attention of most researchers in the last decade due to the fast development in the semiconductor switches which enabled using this technology for long-distance bulk-power delivery and between asynchronous networks [1]. VSC-HVDC even permits connection to dead networks. Pulse width Modulation PWM is the preferred control strategy to such converters for providing high quality ac output voltage to the grid or even to a passive load, [2]. VSC-HVDC systems do not only control active and reactive power independently, but also provide fast and independent voltage regulation to the attached AC system especially for weak grids [3]. The short circuit ratio SCR of an AC grid varies with the change of the grid impedance. The more the grid impedance increases, the AC voltage becomes difficult to control because of higher AC voltage oscillations [4]. For weak AC systems with wide range of varying SCR, converter controllers are difficult to adjust and needs appropriate tuning [5]. The controller design for such systems is a typical robust control design problem which becomes increasingly challenging with the reduction of the AC grid SCR [6]-[10]. The advantages of having robust control solution to weak grids of low SCRs can permit the advances of HVDC application areas and allow power systems for more growth with better dynamic performance without the need for traditionally used expensive solutions such as synchronous condensers SCs and/or static var compensators SVCs [4], [7].

In this paper a decentralized robust controller for a long VSC-HVDC link connected to a weak AC grid is presented. The controller aims at achieving robust stability and superior dynamic performance under large uncertainty in the short circuit ratio SCR of the weak grid. Small-signal modeling and step response analysis are used to confirm the stability of the robust control scheme under wide range of operating conditions and SCR variations. Moreover, the performance of the proposed $\mathcal{H}_\infty$ robust controller is compared with that of a well designed PI controller based system. Modeling and simulation of the proposed control scheme are performed in Matlab environment using the Simulink and Power System Toolboxes.

II. System Description

Fig .1 demonstrates a schematic diagram of the proposed VSC-HVDC transmission system. The system consists of a long DC link cable of a 100 km length connecting two equivalent AC grids through two VSCs. The AC grid of the converter-1 side is a stiff grid whereas that of the converter-2 side is a weak grid. The system parameters are given in

Accepted March 31, 2010.

Table .1. The DC link is monopolar structure and DC capacitors whose sizes are chosen to compromise the level of the DC link voltage ripples and the speed of power transfer capability of the VSC-HVDC transmission system [1].

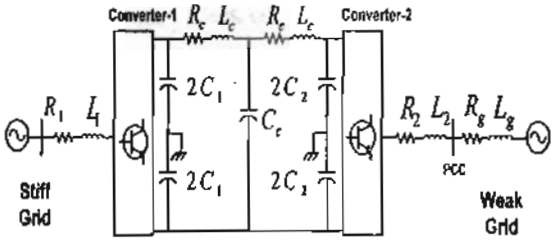

Fig. 1 Schematic diagram of the VSC-HVDC system

Fig. 2 shows the equivalent circuit of the system under study which is shown in Fig. 1. In this paper, it is proposed that converter-1 controller (stiff grid side) is dedicated to control the DC link voltage and the grid reactive power (U_{DC1}, Q_{g1}), whereas converter-2 takes over the control of active and reactive power (P_{g2}, Q_{g2}) of the weak grid. Thereby, for small-signal mathematical modeling, the stiff grid with the converter-1 altogether are modeled by a constant DC voltage source, U_{DCo} while the weak grid side converter-2 is represented by a controlled current source.

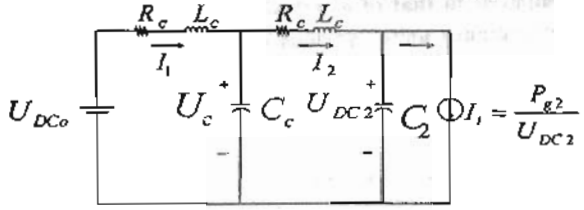

Fig. 2 Equivalent circuit of the VSC-HVDC system given in Fig. 1

Fig. 3 shows the equivalent circuit diagram of the weak grid side; the converter-2 and the model of the phase locked loop PLL that is used to detect the point of common coupling PCC voltage vector magnitude and position. The detected (measured) PCC voltage position is considered equal to the rotating reference frame (dq) in which the system controller is implemented. Fig. 4 shows the phasor diagram of the system variables in the rotating reference frame dq.

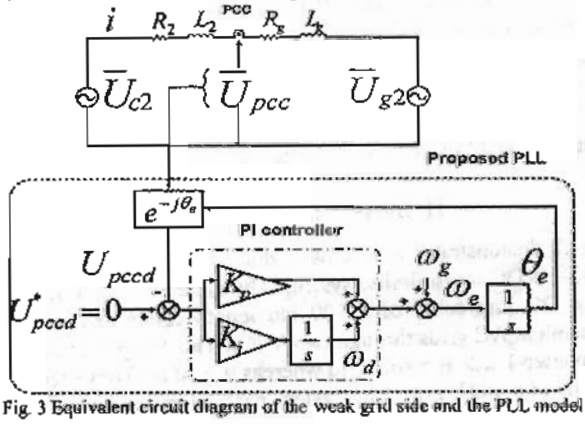

Fig. 3 Equivalent circuit diagram of the weak grid side and the PLL model

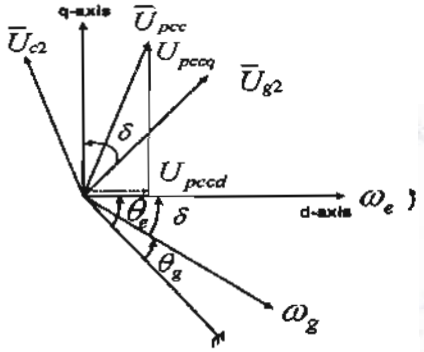

Fig. 4 Phasor diagram of the weak grid side system variables

III. System Modeling

Before proceeding into the mathematical modeling, the following abbreviations are used throughout the analysis: Subscripts *dg* and *qg* are for direct and quadrature components of grid variables. Subscripts *dc* and *qc* are for direct and quadrature components of converter variables. Subscripts *pccd* and *pccq* refer to direct and quadrature components of point of common coupling PCC variables. ω_1 is grid-1 voltage vector angular speed. ω_e, ω_g refer to the angular speed of dq reference frame and the grid-2 voltage vector respectively. θ is the voltage vector position. R_1, R_2 and L_1, L_2 are the equivalent resistances and inductances of the series filters connected to converter-1, 2 respectively. R_g, L_g are the equivalent resistance and inductance of the weak grid. Subscripts g, c, 1 and 2 refer to grid, converter and side-1, 2 variables respectively. i, U, P and Q are current, voltage, active and reactive power respectively. δ is phase angle of the weak grid voltage vector with respect to the synchronous reference frame.

A. Converter-1 side model

As shown in Fig. 2, converter-1 side is modeled by a constant DC voltage source U_{DCo} since high bandwidth controller is used to control the dc link voltage, [1].

B. Converter-2 side model

The model of the VSC-HVDC system proposed in Fig. 1 is nonlinear and thus small-signal model is derived for the purpose of applying the linear control theory for system stability study and controller design. The mathematical model of the equivalent circuit shown in Fig. 2 is derived in two steps. First, the weak grid side model is derived, and then the DC link model including the system controller model is obtained.

C. Weak grid side model

From Fig. 3 and Fig. 4, the weak grid model in a rotating reference frame oriented with the PCC voltage vector can be described as follows:

$$U_{dc2} = R_t i_{dg2} + L_t \dot{i}_{dg2} - \omega_e L_t i_{qg2} + U_{g2} \sin\delta \quad (1)$$

$$U_{qc2} = R_t i_{qg2} + L_t \dot{i}_{qg2} + \omega_e L_t i_{dg2} + U_{g2} \cos\delta \quad (2)$$

$$\dot{\delta} = -k_p U_{pccd} + \omega_d \quad (3)$$

k_p, k_I are the proportional and integral gains of the PLL respectively.

For $k_I \approx 0 \rightarrow \omega_d = 0$

$$\dot{\delta} = -k_p U_{pccd} = \omega_e - \omega_g \quad (4)$$

$$\omega_e = \omega_g + \dot{\delta} = \omega_g - k_p U_{pccd} \quad (5)$$

$$\because U_{pccd} = U_{dc2} - R_2 i_{dg2} - L_2 \dot{i}_{dg2} + \omega_e L_2 i_{qg2}$$
$$= R_g i_{dg2} + L_g \dot{i}_{dg2} - \omega_e L_g i_{qg2} + U_{g2} sin\delta \quad (6)$$

Substituting (6) into (4) for U_{pccd}, one gets:

$$\dot{\delta} = -k_p U_{pccd} = -(k_p R_g) i_{dg2} - (k_p L_g) \dot{i}_{dg2} + (k_p \omega_e L_g) i_{qg2} - k_p U_{g2} sin\delta \quad (7)$$

Substituting from (1) into (7) for $\dot{i}_{dg2}$, yields:

$$\dot{\delta} = -k i_{dg2} - k_p \frac{L_g}{L_t} U_{dc2} - \sigma k_p U_{g2} sin\delta \quad (8)$$

Where $\sigma = 1 - \frac{L_g}{L_t}$, $k = (k_p R_g - k_p \frac{L_g}{L_t} R_t)$

Substituting from (5) into (1) and (2) yields;

$$U_{dc2} = R_t i_{dg2} + L_t \dot{i}_{dg2} - \omega_g L_t i_{qg2} - L_t i_{qg2} \dot{\delta} + U_{g2} sin\delta \quad (9)$$

$$U_{qc2} = R_t i_{qg2} + L_t \dot{i}_{qg2} + \omega_g L_t i_{dg2} + L_t i_{dg2} \dot{\delta} + U_{g2} cos\delta \quad (10)$$

$$\dot{\delta} = -k i_{dg2} - k_p \frac{L_g}{L_t} U_{dc2} - \sigma k_p U_{g2} sin\delta \quad (11)$$

The relation between the converter-2 output voltage and the DC side voltage is given by

$$U_{dc2} = M_{d2} k_2 U_{DC2} \quad , \quad U_{qc2} = M_{q2} k_2 U_{DC2} \quad (12)$$

Where, $k_2 = 1/\sqrt{3}$ and M_{d2}, M_{q2} are the converter-2 direct and quadrature modulation indices.

Substituting from (11), (12) into (9), (10), thereby the grid side model including the PLL model is given by the following three differential equations which involve the grid states (i_{dg2}, i_{qg2} and δ) at any operating point.

$$\dot{i}_{dg2} = -\frac{R_t}{L_t} i_{dg2} + \omega_g i_{qg2} - k i_{dg2} i_{qg2} - U_{g2} sin\delta \left(\frac{1}{L_t} + \sigma k_p i_{qg2}\right) + \frac{k_2}{L_t}(1 - k_p L_g i_{qg2}) M_{d2} U_{DC2} \quad (13)$$

$$\dot{i}_{qg2} = -\frac{R_t}{L_t} i_{qg2} - \omega_g i_{dg2} + k i_{dg2}^2 + \sigma k_p U_{g2} i_{dg2} sin\delta - \frac{U_{g2}}{L_t} cos\delta + \frac{k_2}{L_t} M_{q2} U_{DC2} + \frac{L_g}{L_t} k_p k_2 i_{dg2} M_{d2} U_{DC2} \quad (14)$$

$$\dot{\delta} = -k i_{dg2} - \frac{L_g}{L_t} k_p k_2 M_{d2} U_{DC2} - \sigma k_p U_{g2} sin\delta \quad (15)$$

D. DC link side model

From Fig. 2, it can be seen that the DC link model is a 4th order, since the DC link contains two inductor currents (I_1, I_2) and two capacitor voltages (U_c, U_{DC2}). The set of differential equations describing the DC link is given below.

$$\dot{I}_1 = \frac{1}{L_c}(U_{DCo} - U_c - R_c I_1) \quad (16)$$

$$\dot{U}_c = \frac{1}{C_c}(I_1 - I_2) \quad (17)$$

$$\dot{I}_2 = \frac{1}{L_c}(U_c - U_{DC2} - R_c I_2) \quad (18)$$

$$\dot{U}_{DC2} = \frac{1}{C_2}(I_2 - I_l) = \frac{1}{C_2}\left(I_2 - \frac{P_{g2}}{U_{DC2}}\right)$$
$$\because P_{g2} = \frac{3}{2}(U_{qc2} i_{qg2} + U_{dc2} i_{dg2})$$

Substituting from (12) finally yields

$$\dot{U}_{DC2} = \frac{1}{C_2}\left(I_2 - \frac{3}{2} k_2 (M_{q2} i_{qg2} + M_{d2} i_{dg2})\right) \quad (19)$$

The weak grid model (13) - (15) and the DC link model (16) - (19) together represent the system model under study.

E. Linearized model

It can be noticed that the previous system model is nonlinear. For analyzing the stability of such nonlinear system, it is necessary to linearize the system model around an equilibrium operating point and then apply the linear control theory stability analysis methods. The linearization is based on the Taylor series expansion for nonlinear functions. Assuming a nonlinear function f(x,y,z), its linearized approximation around the steady state (equilibrium) point (x_0, y_0, z_0) is given by:

$$\frac{dx}{dt} = f(x,y,z) \Rightarrow \frac{d\Delta x}{dt} = \frac{\partial f}{\partial x}\Big|_{\substack{y=y_0 \\ z=z_0}} \Delta x + \frac{\partial f}{\partial y}\Big|_{\substack{x=x_0 \\ z=z_0}} \Delta y + \frac{\partial f}{\partial z}\Big|_{\substack{x=x_0 \\ y=y_0}} \Delta z \quad (20)$$

IV. Design of $\mathcal{H}_\infty$ Control Scheme

The proposed control scheme is made up of two separate and independent controllers. The nonlinear controller is used for the stiff grid converter-1 side; it is dedicated to control the DC link voltage and the reactive power, [1]. A multivariable $\mathcal{H}_\infty$ robust controller is proposed to control the weak grid side converter (converter-2). The $\mathcal{H}_\infty$ control approach is adopted for the design of the weak grid system controller in order to achieve robust stability, disturbance rejection and superior dynamic performance under large uncertainty in the short circuit ratio SCR of the weak grid.

Fig. 5 shows the block diagram of the proposed $\mathcal{H}_\infty$ control system of the weak grid side converter. The $\mathcal{H}_\infty$ controller is

used to control the active and the reactive power of the weak grid via controlling their respective current components i_{dg2} and i_{qg2}. The multivariable controller gain (K) can be implemented in state space format with two inputs and two outputs or as four separate transfer functions (K_{11}, K_{12}, K_{21} and K_{22}) forming a transfer function matrix [8].

$$K = \begin{bmatrix} K_{11} & K_{12} \\ K_{21} & K_{22} \end{bmatrix} \quad (21)$$

The outputs of the $\mathcal{H}_\infty$ controller are the dq modulation indices M_{d2}, M_{q2} which are used to generate the switching signals to the converter-2 and the inputs are the dq grid current errors.

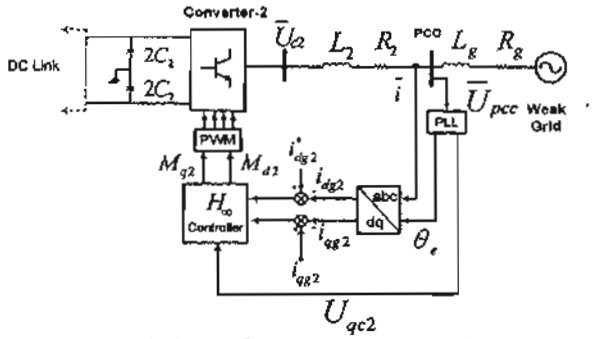

Fig. 5 Block diagram of the proposed $\mathcal{H}_\infty$ control scheme

A. System model uncertainty

The AC system model is considered as an uncertain model since the SCR of the weak AC grid is subjected to wide changes. In this paper, the system model uncertainty is represented by a lumped multiplicative output one as [9].

$$G_p = G(1 + \Delta W_T) \quad (22)$$

Where G_p is the perturbed plant model and G is the nominal plant model. Δ is any stable transfer function which at each frequency, $\|\Delta(s)\| \leq 1 \; \forall\omega$. W_T is the shaping function of the closed loop transfer function.

The relative plant set errors (uncertainty with respect to the nominal plant) $l(j\omega)$ of all valid perturbed plants G_p at different SCRs is represented as

$$l(j\omega) = \max_{G_p \in \Pi} \left| \frac{G_p(j\omega) - G(j\omega)}{G(j\omega)} \right| \quad (23)$$

Where, Π is a set of possible perturbed plant models.

Fig. 6 shows the relative model uncertainty calculated from (23) for a change of the weak grid SCR from 5 to 2. The purpose of Fig. 6 is to find a stable weight filter W_T such that the maximum magnitude of all relative error curves is below this weight for all frequencies.

The multiplicative weight W_T which ensures that the worst case of uncertainty is covered can be found graphically from Fig. 6 as an envelope for the family of transfer functions obtained from (23) as:

$$W_T = 0.000111s + 0.81 \quad (24)$$

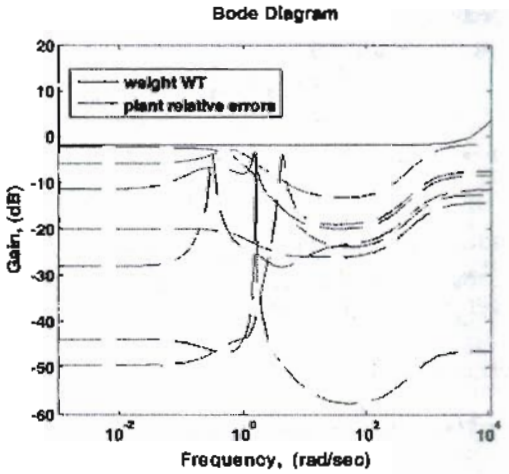

Fig. 6 The shaping weight W_T determined on the basis of relative model uncertainty for SCR change from 5 to 2.

B. Mixed Sensitivity $\mathcal{H}_\infty$ Control Design

The mixed sensitivity approach from $\mathcal{H}_\infty$ theory is used for controller synthesis. In this method of design, the sensitivity (S) and complementary sensitivity (T) of a closed loop plant are shaped by selecting appropriate weights in standard S/T mixed sensitivity $\mathcal{H}_\infty$ design. The weight filters for shaping sensitivity and the complementary sensitivity are W_s and W_T respectively. For any closed loop plant with controller K, If L denotes the open-loop transfer function (L=GK), then the sensitivity and the complementary sensitivity functions can be formulated as, [9]:

$$S = \frac{1}{1+L} \; ; \; T = \frac{L}{1+L} \quad (25)$$

The sensitivity function S is a very good indicator of closed loop performance for both single-input single-output SISO systems and multi-input multi-output MIMO systems.

Actually, the necessary and sufficient condition that must be satisfied by the multivariable $\mathcal{H}_\infty$ controller for robust performance is:

$$\| |W_s S| + |W_T T| \|_\infty < 2 \quad (26)$$

The weight W_s is selected to achieve adequate tracking performance and disturbance rejection. The sensitivity weight filter after [9] is represented as:

$$W_s = \frac{s^2/M + 2\xi\omega_B s/\sqrt{M} + \omega_B{}^2}{s^2 + 2\omega_B s\sqrt{A} + A\omega_B{}^2} \quad (27)$$

Thereby, the selected (tuned) W_s filter parameters are:

$$M = 500 \; ; \; \xi = 2 \; ; \; A = 10^{-4} \; ; \; \omega_B = 200$$

Fig. 7 shows the frequency response of the chosen weights W_s and W_T with the sensitivity S and the complementary sensitivity T of the system. It can be seen that the condition for robust performance (26) is satisfied.

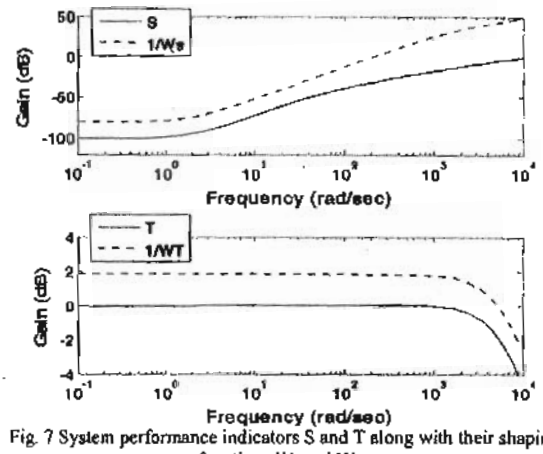

Fig. 7 System performance indicators S and T along with their shaping functions W_s and W_T.

The robust controller in (21) that satisfies (26) is known as mixed sensitivity $\mathcal{H}_\infty$ controller, and is obtained using the Matlab robust control toolbox using the linearized system model and the chosen weight filters W_s, W_T, (24) and (27).

V. Design of PI Control Scheme

Fig. 8 shows the block diagram of the decoupled PI current control scheme for the weak grid side converter. Like the $\mathcal{H}_\infty$ controller, the PI controller is used to control the active and reactive power of the weak grid (P_{g2}, Q_{g2}) through controlling their respective current components i_{qg2}, i_{dg2}. The outputs of the PI control loops are the dq modulation indices M_{d2}, M_{q2}.

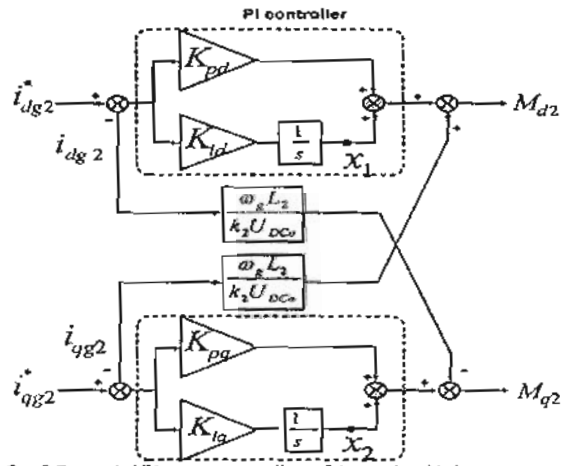

Fig. 8 Decoupled PI current controllers of the weak grid side converter

A. Modelling of PI control Scheme

Integrating the PI controller model with the system model adds two new states (x_1, x_2) to the mathematical model of the control system. The PI controller model shown in Fig. 8 can be described by the differential equations below.

$$\dot{x}_1 = (i^*_{dg2} - i_{dg2})K_{Id} \quad (28)$$

$$\dot{x}_2 = (i^*_{qg2} - i_{qg2})K_{Iq} \quad (29)$$

$$M_{d2} = (i^*_{dg2} - i_{dg2})K_{pd} + x_1 + hi_{dg2} \quad (30)$$

$$M_{q2} = (i^*_{qg2} - i_{qg2})K_{pq} + x_2 - hi_{qg2} \quad (31)$$

Where, $h = \dfrac{\omega_g L_2}{k_2 U_{DCo}}$

Substituting (30), (31) into (13 – 19), one gets the final differential equations of the overall PI control system model, which after linearization based on (20) are expressed in the well known state space form as:

$$\Delta\dot{x} = A_o\,\Delta x + B_o \Delta u \quad (32)$$

$$\Delta y = C_o \Delta x \quad (33)$$

$$\Delta x = [\Delta i_{dg2}\ \Delta i_{qg2}\ \Delta\delta\ \ \Delta I_1\ \Delta U_c\ \Delta I_2\ \Delta U_{DC2}\ \Delta x_1\ \Delta x_2]^T$$

$$\Delta u = [\Delta i^*_{dg2}\ \Delta i^*_{qg2}]^T\ , \qquad \Delta y = [\Delta i_{dg2}\ \Delta i_{qg2}]^T$$

The state space model (32) - (33) is implemented using Matlab control toolbox and used to choose the gains of the PI controllers through step response analysis.

B. Choice of the PI controller gains

The PI controller parameters K_{pd}, K_{Id}, K_{pq} and K_{Iq} are designed to satisfy two performance objectives, 1) overshoot of less than 10%, 2) settling time inside the 2% band error lower than 0.02 sec.

The linearized state space model of the PI control system is used to study the system step response dynamics using the Matlab control toolbox. Figs. 9 and 10 show the PI control system closed-loop transfer function response for a step change in the active and reactive currents i_{qg2}, i_{dg2} respectively with different PI controllers gains at the nominal SCR = 5 and for an equilibrium operating point $P_{g2} = -0.6\,pu, Q_{g2} = 0.6\,pu$. The proportional gains are set constant at $K_{pd} = K_{pq} = 0.003$ and the system step responses are recorded for different integral gains K_{Id}, K_{Iq}, changing from 1 to 7. It is evident that the system response with higher integral gains results in higher overshoots. Therefore, from the results shown in Figs. 9 and 10, the PI controllers gains of both control loops (active and reactive power loops) that satisfy the desired response are chosen as:

$$K_{pd} = K_{pq} = 0.003\ \ \&\ \ K_{Id} = K_{Iq} = 1 \quad (34)$$

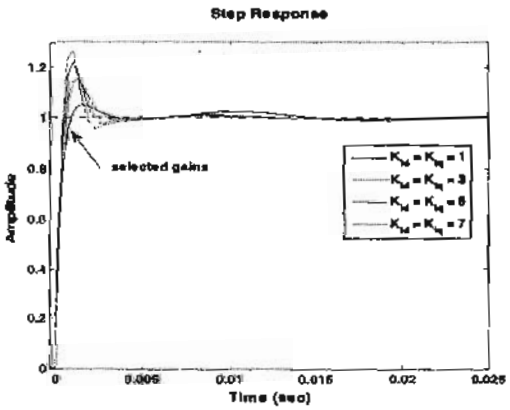

Fig. 9 System step response to a step change of active power current component i_{q2} with different integral PI controllers gains for SCR = 5

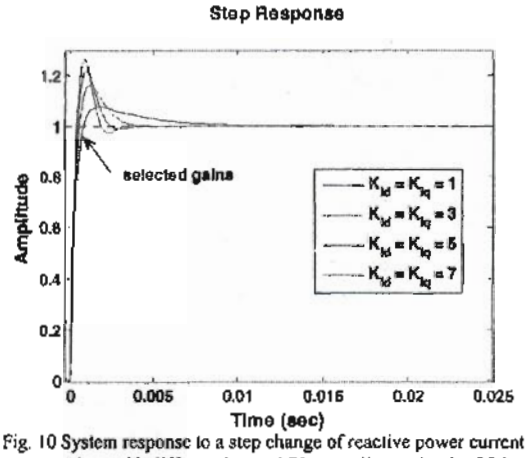

Fig. 10 System response to a step change of reactive power current component i_{dg2} with different integral PI controllers gains for SCR = 5

It should be noted from Figs. 9, 10 that the dynamics of the two current control loops are different although the PI controllers' gains used are the same. The response of the current i_{qg2} shown in Fig. 9 is more oscillatory, which indicates a higher order closed loop transfer function. The reason is that the exchanged active power between the AC grid and its attached converter travels via the DC link (cable) to the other converter on the other side of the DC link involving the DC link model into the overall closed loop dynamics of the current i_{qg2} control channel. On contrary, the reactive power is locally exchanged between the grid side converter and its AC grid without crossing the DC link. Therefore, as the closed loop dynamics of the currents i_{dg2} and i_{qg2} control channels are different, it is proposed to use PI controllers of different gains for controlling the active and reactive powers and to match the dynamics of each individual control loop.

Fig. 11 shows the step response for the reactive power current component i_{dg2} with different PI controllers' gains. It is clear that the transient response is better and with smaller settling time in case of using relatively higher integral gain for the reactive power control loop.

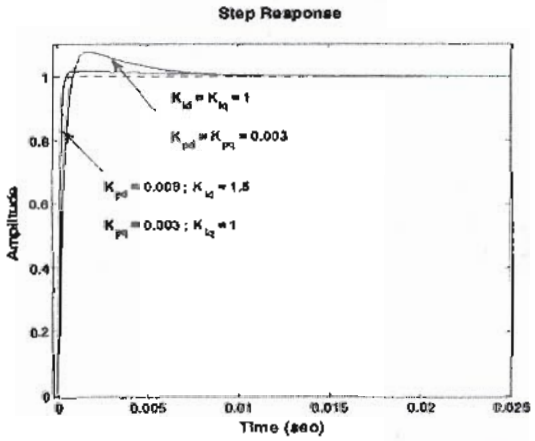

Fig. 11 System response to a step change of reactive power current component i_{dg2} with different PI gains of both control loops for SCR = 5

Finally, the PI controllers' gains of both control loops are chosen as:

$$K_{pd} = 0.009\,,\ K_{id} = 1.5\ \&\ K_{pq} = 0.003\,,\ K_{iq} = 1 \quad (35)$$

To this extent, the $\mathcal{H}_\infty$ controller and its opponent PI controller are designed to provide the specified dynamic characteristics. In the next section, the dynamic performance of the two control systems is compared.

VI. Simulation Results and Discussion

This section demonstrates a set of simulation test results to verify the effectiveness of the proposed $\mathcal{H}_\infty$ controller under large uncertainty in the weak grid SCR. The $\mathcal{H}_\infty$ and the PI control schemes are modeled and simulated using the Matlab Simulink toolbox. The systems are subjected to a reduction of the SCR for a range from 5 to 2. The SCR of the AC grid is varied by changing the AC system parameters (R_g, L_g) while the ratio between $X_g(\omega_e L_g)$ and R_g is assumed to be constant, i.e. $(X_g/R_g = 10)$. The parameters of the AC system under study are listed in Table.1. It should be noted that all the demonstrated results are in pu.

A. Active power step change: SCR = 5 test case

Figs. 12 and 13 demonstrate tests for step change in the active power current component i_{qg2} for a higher SCR = 5 and at two different equilibrium points of operation where in Fig. 12 the step change is around a positive active power of 0.6 pu while Fig. 13 is for a negative active power of -0.6 pu. It should be noted that the reactive power is set constant and equal to 0.6 pu. From the two figures, it can be seen that at the moments of step changes (0.1s, 0.15s), the proposed $\mathcal{H}_\infty$ controller provides fast transient response and also guarantees decoupled control for both active and reactive power current components in comparison to the PI controller case.

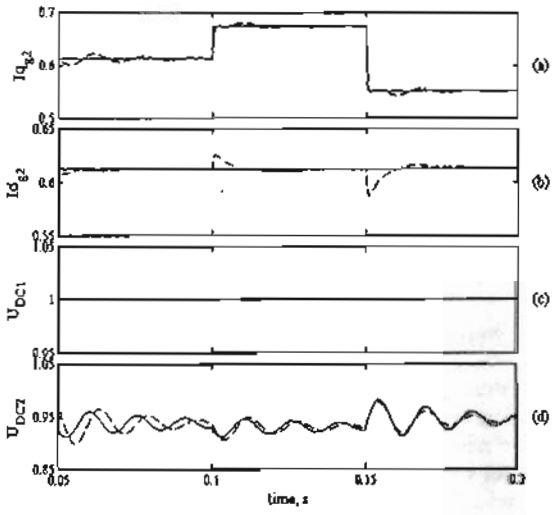

Fig. 12 System step response at a positive active power current component i_{qg2} for SCR = 5. Solid lines are for the proposed H_∞ controller and dashed lines are for PI controller.

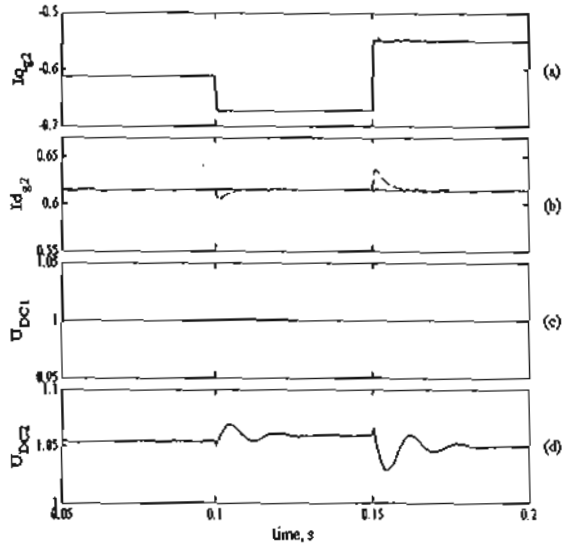

Fig. 13 System step response at a negative active power current component i_{qg2} for SCR = 5. Solid lines are for proposed H_∞ controller and dashed lines are for PI controller.

B. Active power step change: SCR = 2 test case

The two control systems are subjected to the same step change tests as performed in the previous section but for a lower SCR = 2. Figs. 14, 15 show the system behavior under such tests. It is evident from the results that the proposed $\mathcal{H}_\infty$ controller provides robust performance at reduced system strength (SCR), where the controller still preserves its fast transient response. Whereas, the PI controller suffers from relatively higher overshoots with long settling times after the moments of step changes.

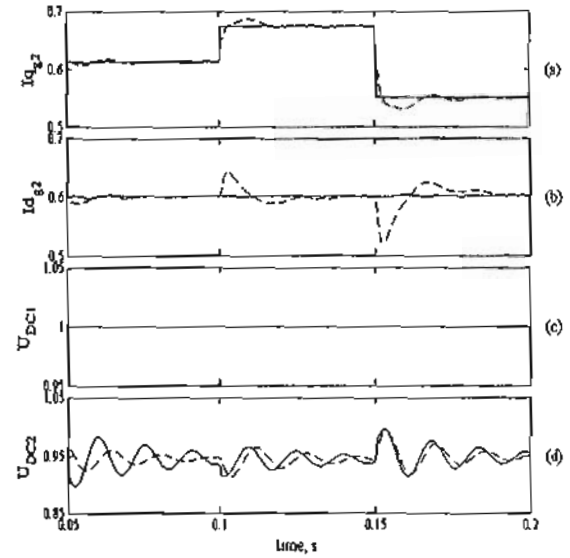

Fig. 14 System step response at a positive active power current component i_{qg2} for SCR = 2. Solid lines are for proposed $\mathcal{H}_\infty$ controller and dashed lines are for PI controller.

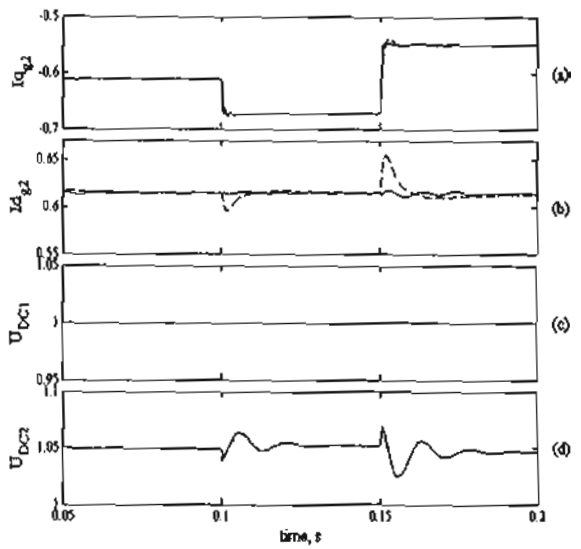

Fig. 15 System step response at a negative active power current component i_{qg2} for SCR = 2. Solid lines are for proposed $\mathcal{H}_\infty$ controller and dashed lines are for PI controller.

VII. Conclusions

A multivariable decentralized robust $\mathcal{H}_\infty$ controller for a long VSC-HVDC transmission line connected to a weak AC grid has been designed and tested. The VSC-HVDC system is used to connect a weak AC gird to a strong power system using a long DC link. Small-signal modeling, step response study and simulation work have been carried out to investigate the proposed control system stability, dynamic performance and robustness to SCR variation.

The $\mathcal{H}_\infty$ controller performance has been compared to a well designed PI controller based system. The $\mathcal{H}_\infty$ and the PI type control systems are modeled and simulated in Matlab environment using the Simulink Toolbox. The test results are obtained at different equilibrium points and at two different SCRs of 5 and 2. The results are compared and the $\mathcal{H}_\infty$ type is found superior in comparison to the PI type based control system for a wide range of SCR uncertainty.

Table.1 System parameters values

Description	Symbol		Value
Grid voltage (line to line)	U_g		10 KV
Series filter resistance	R_1,R_2		0.1 Ω
Series filter inductance	L_1,L_2		2 mH
Weak AC grid resistance	SCR = 5	R_g	0.33 Ω
	SCR = 2	R_g	0.83 Ω
Weak AC grid inductance	SCR = 5	L_g	10.6 mH
	SCR = 2	L_g	26.5 mH
DC link capacitors	C_1,C_2		200 μF
DC cable resistance	2Rc		3.7 Ω
DC cable inductance	$2L_c$		27 mH
DC cable capacitance	C_c		34 μF
Converter rated capacity	-		10 MVA
Rated DC link voltage	U_{DCo}		20 V

VIII. References

[1] Mohamed Rashed, Sayed M. Abo El-Anwar and Fathi M. H. Youssef, "Nonlinear control scheme for VSC-HVDC transmission systems", *12th International Middle-East Power Systems Conference MEPCON 2008, Aswan, Egypt, March, 2008, pp. 486-491.*

[2] F. Schettler, H. Huang, N. Christl, "HVDC transmission systems using voltage sourced converters design and application", *IEEE, Power Engineering Society Summer Meeting, Conference, vol 2, 2000, pp. 715-720.*

[3] Wenze Liu, Zexiang Cai, "Model Analysis and Robust Control Design of VSC-HVDC Converter with dq0 Axis", *IEEE, 3rd International Conference on Electric Utility Deregulation and Power Technologies, 6-9 April, 2008, pp. 1792-1796.*

[4] Jovcic D, "Control of high voltage DC and flexible AC transmission systems", *PhD Thesis, University of Auckland, New Zealand, December 1999.*

[5] Kala Meah, "A self coordinating parallel multi-PI control scheme for an HVDC transmission system to accommodate a weak AC system", *PhD Thesis, Wyoming University, Laramie, Wyoming, December, 2007.*

[6] Martyn Durrant, Herbert Werner, Keith Abbott, "A comparison of LMI and GA based robust controller designs for VSC HVDC", *45th IEEE Conference on Decision & Control, San Diego, USA, December, 2006, pp. 3990-3995.*

[7] Jorge Wilson Gonzalez , Christian Weindl , Gerhard Herold , Dietmar Retzmann, Hugo A. Cardona, Idi A. Isaac and Gabriel J. Lopez., "Feasibility of HVDC for very weak AC systems with SCR below 1.5", *IEEE 12th International Power Electronics and Motion Control Conference, 2006, pp. 1522-1527.*

[8] Aten, M. and Werne, H., "Robust multivariable control design for HVDC back to back schemes", *IEE Proc.-Gen. Transm. Distrib., Vol 150, No. 6, November, 2003, pp. 761 - 767.*

[9] Skogestad, S., and Postlethwaite, I, "Multivariable feedback control", *(John Wiley, Chichester 1996).*

[10] Jovcic. D., and Sternberger R., "Robust controller design for a multilevel cascaded STATCOM", *IEEE, Power and Energy Society General Meeting, Conference proceeding, 2008, pp. 1-6.*